AGU100 ADVANCING EARTH AND SPACE SCIENCE

JGR

Journal of Geophysical Research: Space Physics

RESEARCH ARTICLE

10.1002/2017JA025136

Key Points:

- While underlying field-aligned currents (FACs) vary with season, currents from substorm activity show little seasonal variability
- FACs increase in the postnoon and premidnight quadrants before onset, with faster nightside increases occurring after dayside increases
- The time profile of substorm field-aligned currents and SML agrees with a resistive-capacitive model of the current system

Correspondence to:
C. Forsyth,
colin.forsyth@ucl.ac.uk

Citation:
Forsyth, C., Shortt, M., Coxon, J. C., Rae, I. J., Freeman, M. P., Kalmoni, N. M. E., et al. (2018). Seasonal and temporal variations of field-aligned currents and ground magnetic deflections during substorms. *Journal of Geophysical Research: Space Physics*, *123*, 2696–2713. https://doi.org/10.1002/2017JA025136

Received 20 DEC 2017
Accepted 9 MAR 2018
Accepted article online 25 MAR 2018
Published online 19 APR 2018

Seasonal and Temporal Variations of Field-Aligned Currents and Ground Magnetic Deflections During Substorms

C. Forsyth[1], M. Shortt[1], J. C. Coxon[2], I. J. Rae[1], M. P. Freeman[3], N. M. E. Kalmoni[1], C. M. Jackman[2], B. J. Anderson[4], S. E. Milan[5], and A. G. Burrell[6]

[1]Mullard Space Science Laboratory, UCL, Dorking, UK, [2]Department of Physics and Astronomy, University of Southampton, Southampton, UK, [3]British Antarctic Survey, Cambridge, UK, [4]John Hopkins University Applied Physics Laboratory, Laurel, MD, USA, [5]Department of Physics and Astronomy, University of Leicester, Leicester, UK, [6]William B. Hanson Center for Space Sciences, University of Texas at Dallas, Dallas, TX, USA

Abstract Field-aligned currents (FACs), also known as Birkeland currents, are the agents by which energy and momentum are transferred to the ionosphere from the magnetosphere and solar wind. This coupling is enhanced at substorm onset through the formation of the substorm current wedge. Using FAC data from the Active Magnetosphere and Planetary Electrodynamics Response Experiment and substorm expansion phase onsets identified using the Substorm Onsets and Phases from Indices of the Electrojet technique, we examine the Northern Hemisphere FACs in all local time sectors with respect to substorm onset and subdivided by season. Our results show that while there is a strong seasonal dependence on the underlying FACs, the increase in FACs following substorm onset only varies by 10% with season, with substorms increasing the hemispheric FACs by 420 kA on average. Over an hour prior to substorm onset, the dayside currents in the postnoon quadrant increase linearly, whereas the nightside currents show a linear increase starting 20–30 min before onset. After onset, the nightside Region 1, Region 2, and nonlocally closed currents and the SuperMAG AL (SML) index follow the Weimer (1994, https://doi.org/10.1029/93JA02721) model with the same time constants in each season. These results contrast earlier contradictory studies that indicate that substorms are either longer in the summer or decay faster in the summer. Our results imply that, on average, substorm FACs do not change with season but that their relative impact on the coupled magnetosphere-ionosphere system does due to the changes in the underlying currents.

Plain Language Summary Earth is surrounded by electrical currents flowing in space. These currents, which can be 10,000 times greater than domestic electrical supplies, can flow along the Earth's magnetic field and into the upper atmosphere and are linked to aurora. The size of this current depends on atmospheric conditions, with the upper atmosphere being a better conductor when it is sunlit, and the interaction between particles flowing from the Sun and the Earth's magnetic field. During space weather events known as substorms, which happen several times per day on average, the aurora brightens massively and the currents flowing into the upper atmosphere increase. Using data from the Iridium communications satellites, the increase in this current can be measured. While the strength of the day-to-day current varies with season, as expected from simple models of the system, the increases due to these space weather events are the same throughout the year.

1. Introduction

Field-aligned currents (FACs) are the key mechanism by which energy and momentum connect the magnetosphere and ionosphere. On a large scale, FACs form two regions (Iijima & Potemra, 1976, 1978): poleward of the auroral oval, the Region 1 currents flow into the ionosphere on the dawnward side and out of the ionosphere on the duskward side, closing across the polar cap or the auroral oval; equatorward of the auroral oval, the Region 2 currents flow into the ionosphere on the duskward side and out of the ionosphere on the dawnward side. The Region 1 and Region 2 currents predominantly close via ionospheric Pedersen currents across the auroral oval but can also close across the polar cap (Fujii et al., 1981; Le et al., 2010) and via Hall currents when ionospheric conductivity is nonuniform. These large-scale current systems link to the magnetospheric plasma convection of the Dungey Cycle (see Milan et al., 2017, for a recent review) and appear as both a statistical average (Iijima & Potemra, 1978) and in snapshots of the current systems (Anderson et al., 2008).

The substorm cycle modifies and enhances the global currents associated with the Dungey Cycle (see Kepko et al., 2015, for a recent review). Enhanced rates of dayside reconnection during the growth phase open magnetospheric magnetic flux. The subsequent enhancement in polar cap convection is expected to spread from the dayside toward the nightside (Cowley & Lockwood, 1992) with an associated enhancement in the large-scale FACs. Observations have shown that the dayside currents are enhanced soon after the arrival of southward interplanetary magnetic field (IMF) at the magnetopause followed by the nightside currents some 40–70 min later (Anderson et al., 2014; He et al., 2014). At (or soon following) substorm expansion phase onset, the nightside FACs are enhanced and an equivalent Region 1-type current system, known as the "substorm current wedge," forms from the diversion of cross-tail currents. This forms a new FAC system (Akasofu & Chapman, 1972; Mcpherron et al., 1973) or enhances the magnitude of and moves existing FACs (Friedrich & Rostoker, 1998; Rostoker, 1974; Rostoker & Friedrich, 2005). Recent studies have suggested that the substorm current wedge could also include a R_2-type current system (Coxon et al., 2014a; Liu et al., 2016; Ritter & Luhr, 2008; Sergeev et al., 2014). Some 15–30 min after the substorm onset, the currents begin to reduce toward their presubstorm levels in a period known as the recovery phase.

While examining the low-altitude FAC using single or multispacecraft missions has provided new insights into the small-scale structuring of the FACs (e.g., Dunlop et al., 2015; Forsyth et al., 2014; Gjerloevet al., 2011; Lühr et al., 2015), the global FAC system has previously only been accessible through statistical averaging of multiple polar passes (e.g., Gjerloev & Hoffman, 2002; Iijima & Potemra, 1978; Juusola et al., 2009, 2014; Huang et al., 2017; Papitashvili et al., 2002; Stauning, 2002; Stauning et al., 2005; Wang et al., 2005; Weimer, 2001). Since 2012, the Active Magnetosphere and Planetary Electrodynamics Response Experiment (AMPERE; Anderson et al., 2000, 2002, 2014; Green et al., 2006; Waters et al., 2001) has provided near-continuous estimates of the large-scale polar FAC systems by combining data from the 66 satellites that comprise the Iridium constellation.

Data from AMPERE have provided new insights into the dynamics of the global FACs during substorms (see recent review by Coxon et al., 2018). As expected, the FACs increase after substorm onset (Clausen, Milan, et al., 2013; Clausen et al., 2013; Sergeev et al., 2014; Sergeev et al., 2014), with substorms at lower latitudes generally being associated with larger FACs (Coxon et al., 2014b). Furthermore, the Region 1 and Region 2 current systems move in conjunction with the opening and closing of magnetic flux, determined using the location of the R_1 current system as a proxy for the open-closed field line boundary (Clausen et al., 2012, 2013, 2013). The Region 1 and Region 2 currents are also moderately correlated with both dayside reconnection and geomagnetic activity (Coxon et al., 2014a). Interestingly, the substorm current wedge does not appear as a principal component of the FACs (Milan et al., 2015), although it can be revealed through differencing techniques (Clausen et al., 2013). While the large-scale currents increase after substorm onset, AMPERE has also revealed that FACs decrease in a localized region close to the onset latitude and magnetic local time (MLT) just prior to onset, in keeping with the phenomenon of auroral dimming (Coxon et al., 2017; Murphy et al., 2012).

The FACs that couple to each hemisphere vary seasonally (Coxon et al., 2016; Fujii et al., 1981; Ohtani et al., 2005). This effect is largely dominated by the seasonal variations in ionospheric conductivity due to illumination by sunlight. However, studies of the seasonal variability of substorms show differing results. Chua et al. (2004) showed that the auroral hemispheric power, calculated from auroral images, decayed more quickly during the summer and that the peak power was highest near the equinoxes. Tanskanen et al. (2011) reported that the ground magnetic signature of substorms was most intense and longer lasting during the summer. By directly examining the FACs associated with substorms, we aim to resolve this apparent inconsistency.

The time profile of the substorm current system has previously been modeled based on the premise that the coupled magnetosphere-ionosphere system acts as a resistive-capacitive circuit (Weimer, 1994). This model has been shown to fit the average ground magnetic perturbations during substorms. However, these perturbations are not a direct measure of the FACs and can be complicated by changes in the ionospheric Hall and Pedersen conductivities and the formation of Cowling channels in response to the substorm current wedge (Cowley, 2000). By directly measuring the FACs above the ionosphere, we can remove this ambiguity and test whether or not the Weimer (1994) model fits the observed current systems.

2. Methodology

In this study, we use the FACs from the Northern Hemisphere from AMPERE combined with information about substorm activity from the Substorm Onsets and Phases from Indices of the Electrojet technique (SOPHIE; Forsyth et al., 2015). We compare the observed field-aligned currents with the SuperMAG *AU* and *AL* indices (SMU and SML; Newell & Gjerloev, 2011; Gjerloev, 2012).

2.1. Field-Aligned Currents From AMPERE

AMPERE provides continuous monitoring of the global field-aligned current system coupling the ionosphere to the magnetosphere through measurements of the low-altitude perturbation magnetic field made by magnetometers on board the Iridium® telecommunications constellation (Anderson et al., 2000, 2002, 2014; Green et al.,2006; Waters et al.,2001). The Iridium constellation consists of 66 spacecraft in six equally spaced orbital planes, providing 2 hr local time separation. The magnetic field data from the spacecraft are processed using a spherical harmonic inversion of a potential formalism from which the FACs are derived (Green et al., 2006; Waters et al., 2001). AMPERE provides the FACs in the polar regions on a grid of 1 hr of magnetic local time and 1° of magnetic latitude in the Altitude Adjusted Corrected Geomagnetic coordinate system at 780 km. These data are provided at 2 min resolution, although it should be noted that 10 min of spacecraft data are required to build up each field-aligned current map. As such, there is an inherent assumption that the currents and magnetic field perturbations do not significantly change over the 10 min integration time. In this study, we use the end of each data integration window as the time tags for the FAC data, as per Anderson et al. (2014).

In order to analyze the FACs, we reduce the AMPERE data set into total upward (*U*) and downward (*D*) FACs in each MLT sector. The observed upward and downward current densities in each grid cell are multiplied by the area of the cell to recover the total current. These currents are then integrated between 60° and 90° magnetic latitudes, providing the total upward and downward current for each hour of MLT. Due to the sensitivity of the magnetometers on board the Iridium constellation, and the spherical harmonic fitting technique used, FACs with a magnitude less than 0.2 $\mu A/m^{-2}$ are rejected and not included in our integration (Anderson et al., 2014; Clausen et al., 2012).

FACs occur across a range of spatial scales. Small-scale FACs, with widths of a few kilometers, are often reported to have much larger current densities than large-scale currents and may play an important role in magnetosphere-ionosphere coupling (e.g., Lühr et al., 2004; McGranaghan et al., 2017; Neubert & Christiansen, 2003; Rother et al., 2007; Watermann et al., 2009; Wu et al., 2017). However, these currents tend to be localized (e.g., Lühr et al., 2015) and thus the total current carried may be relatively small. Furthermore, there are outstanding questions as to whether the magnetic field perturbations used to calculate these small-scale currents are from time-stationary FACs or from wave activity (Forsyth et al., 2017; Gjerloev et al., 2011; Miles et al., 2018; Pakhotin et al., 2018). In contrast, FACs with scales of the order of hundreds of kilometers tend to be much better defined. AMPERE combines data from 12 local times taken over 10 min using a spherical harmonic fit to calculate these large-scale current systems. As such, AMPERE cannot diagnose FACs with scales below a few degrees latitude and a few hours of MLT, instead returning the net current flowing in each observation cell. However, AMPERE is currently the only data set that provides near-instantaneous in situ observations of the global current system, as opposed to climatological analysis, and thus provides a new opportunity to analyze the dynamics of the large-scale current system.

2.2. Substorm Onsets From SOPHIE

In order to examine the variation of the FACs with respect to substorm activity, substorm onsets are identified using the SOPHIE technique (Forsyth et al., 2015). This technique uses data from the SuperMAG project that amalgamates observations from ~110 ground-based magnetometers onto a common time base and with a common baselining technique (Gjerloev, 2012; Newell & Gjerloev, 2011). The SuperMAG *AL* (SML) index is then generated, along with the MLT and magnetic latitude of the corresponding magnetometer. From this index, SOPHIE identifies substorm expansion and recovery phases and possible growth phase intervals by identifying those times when the gradient of SML exceeds a specified percentile of the yearly distribution of gradients. Here we use a percentile of 75%, which was shown to produce onsets with good agreement to auroral onset lists. The SOPHIE technique does not force expansion phases to follow potential growth phases, and as such, multiple onset or compound substorms can be readily identified. SOPHIE also

identifies those events in which the SuperMAG *AU* (SMU) index is enhanced to a level comparable to the SML, suggesting that the SMU is elevated by enhanced magnetospheric convection rather than the substorm electrojet (Kamide et al., 1996).

In this study, we examine the substorm currents from those substorm expansion phases directly preceded by a possible growth phase (excluding multiple or compound substorms), although we do not dictate the length of this preceding growth phase. We also reject any events that show signatures of enhanced convection as opposed to substorm activity, as described above. Given that SML is generated from a network of magnetometer stations, the magnetic local time (MLT) of the station providing the SML (and thus where the westward ionospheric current is strongest) at each epoch can be determined. We restrict our event list to events in which the location of the active SML station at substorm onset was between 20 and 04 MLT such that ionospheric current activity is on the nightside. Between 1 January 2010 and 1 January 2013 this provides 2,434 substorm onsets, an average of three per day.

2.3. Data Processing Using Superposed Epoch Analysis

In this study, we examine the FAC from AMPERE along with the SML and SMU auroral indices. Throughout, we perform superposed epoch analyses taking substorm onset from SOPHIE as $t = 0$ min. At each preceding and subsequent time point, we take the mean value of the distribution of observed values.

3. Results

3.1. Observational Framework

Large-scale FACs are often described in terms of the Region 1 and Region 2 currents formulated by Ijima and Potemra (1976, 1978). The downward Region 1 currents flow into the ionosphere at high latitudes on the dawnside, coupling across the auroral region to the upward Region 2 currents on the dawnside and coupling across the polar cap to the upward Region 1 currents on the duskside. Using this framework, we define the following currents:

$$I_{1,\mathrm{MLT}} = \mathrm{MAX}\{|U_{\mathrm{MLT}}|, |D_{\mathrm{MLT}}|\} \tag{1}$$

$$I_{2,\mathrm{MLT}} = \mathrm{MIN}\{|U_{\mathrm{MLT}}|, |D_{\mathrm{MLT}}|\} \tag{2}$$

where U_{MLT} and D_{MLT} are the upward and downward currents in a given MLT sector and $I_{1,\mathrm{MLT}}$ and $I_{2,\mathrm{MLT}}$ are the Region 1 and Region 2 currents in given MLTs. The total Region 1 and Region 2 currents flowing into the Northern Hemisphere are then defined as

$$R_1 = \frac{\sum I_{1,\mathrm{MLT}}}{2}; R_2 = \frac{\sum I_{2,\mathrm{MLT}}}{2} \tag{3}$$

The division by 2 accounts for the fact the summing over all sectors incorporates both the upward and downward components of the Region 1 and Region 2 currents.

To a first approximation, the ionospheric current flowing across the auroral oval in any given local time sector is the equal to the $I_{2,\mathrm{MLT}}$. The difference between $I_{1,\mathrm{MLT}}$ and $I_{2,\mathrm{MLT}}$ is thus an ionospheric current flowing into or out of that local time sector. This could manifest as the cross-polar cap current or an enhancement in the electrojets. The nonlocally closed ionospheric current is thus given as

$$I_{i,\mathrm{MLT}} = I_{1,\mathrm{MLT}} - I_{2,\mathrm{MLT}} \tag{4}$$

and similar to R_1 and R_2, the combined polar cap and electrojet currents are

$$R_i \frac{\sum I_{1,\mathrm{MLT}}}{2} \tag{5}$$

Figure 1 shows a schematic of this framework.

Farther to the Region 1 and Region 2 frameworks described above, we consider the global variations in the FACs to be described fixed "baseline currents" ($B_{U,\mathrm{MLT}}$, $B_{D,\mathrm{MLT}}$) and a temporally varying "substorm currents" ($S_{U,\mathrm{MLT}}$, $S_{D,\mathrm{MLT}}$):

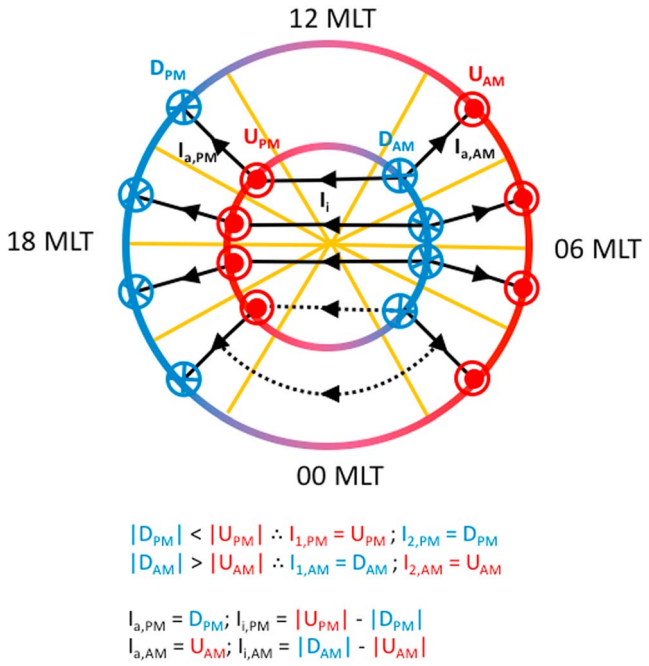

Figure 1. Schematic showing the observational framework of current systems used in this study. Red indicates upward FAC, and blue indicates downward FAC current. The inner and outer rings represent the Region 1 and Region 2 currents. The black lines show ionospheric currents. In this example, the nonlocally closed ionospheric currents flow across the polar cap to the opposite MLT sector (solid lines) or across the polar cap and through the electrojet (dashed lines).

$$U_{\mathrm{MLT}} = B_{U,\mathrm{MLT}} + S_{U,\mathrm{MLT}}(t); D_{\mathrm{MLT}} = B_{D,\mathrm{MLT}} + S_{D,\mathrm{MLT}}(t) \quad (6)$$

We define the underlying currents as the median FAC in the hour prior to substorm onset.

It is often useful to combine FACs in different sectors for comparison. To that end, we identify different sectors using the following subscripts: dawnside (00–12 MLT) is *am*, duskside (12–24 MLT) is *pm*, dayside (06–18 MLT) is *d*, nightside (18–06 MLT) is *n*, postmidnight quadrant (00–06 MLT) is *PoM*, prenoon quadrant (06–12 MLT) is *PrN*, postnoon quadrant (12–18 MLT) is *PoN*, and premidnight quadrant (18–24 MLT) is *PrM*.

3.2. Seasonal Variations in Substorm FAC

Previous studies have shown that FACs vary with season (Coxon et al., 2016). The total FAC flowing through the summer hemisphere is greater than that flowing through the winter hemisphere. Here we investigate whether or not there is a seasonal effect on the substorm component of this current system. Our results are summarized in Table 1.

Figure 2 shows the results of the superposed epoch analysis of the total upward (top) and downward (middle) FAC in each MLT sector (*x* axis) with respect to substorm onset (*y* axis). The four columns show the FACs separated by season, taken to be 45 days on either side of the solstices or equinoxes. The bottom row of Figure 2 shows $R_{1\text{-}pm}$ (black solid), $R_{1\text{-}am}$ (black dashed),$R_{2\text{-}pm}$ (red solid), and $R_{2\text{-}am}$ (red dashed) currents. Also shown is R_i (blue).

Figure 2 shows a seasonal variation in the Northern Hemisphere FACs, with the FACs being strongest in the summer and weakest in the winter. Comparing similar traces in each of the bottom panels of Figure 2 shows that the strengths of the currents before onset vary with season. Table 1 shows that the dayside baseline currents $B_{U\text{-}d}$ and $B_{D\text{-}d}$ differ by more than 550 kA between the summer and winter, whereas substorm currents S_U and S_D vary by less than 40 kA. During the summer, the largest FACs are on the dayside, whereas in the winter the largest FACs appear on the nightside after substorm onset. This seasonal effect is also evident in R_1 and R_2 (Figure 2, bottom row). On average, R_1 is 395 kA (50%) stronger in summer than in the winter, while R_2 is only 277 kA (41.7%) stronger in summer than in the winter. As such, the Region 1 currents have a greater seasonal variability than the Region 2 currents.

Table 1
Seasonal Properties and Changes in FAC Systems

	Maximum value				Mean value			
	Spring	Summer	Autumn	Winter	Spring	Summer	Autumn	Winter
Region 1 (R_1; kA)	1,102	1,343	1,168	890	978	1,183	1,036	788
Region 2 (R_2; kA)	906	1,050	959	753	795	942	856	665
Polar cap and electrojet currents (R_i; kA)	221	307	221	160	183	241	178	123
Region 1 dawn-dusk asymmetry ($R_{1\text{-am}}/R_{1\text{-pm}}$)	1.27	1.1	1.12	1.19	1.2	1.04	1.05	1.13
Region 2 dawn-dusk asymmetry ($R_{2\text{-am}}/R_{2\text{-pm}}$)	1.23	1.09	1.08	1.27	1.15	1.02	0.99	1.19
	Upward FAC				Downward FAC			
	Spring	Summer	Autumn	Winter	Spring	Summer	Autumn	Winter
Underlying dayside FAC ($B_{U\text{-}d}$, $B_{D\text{-}d}$; kA)	710	1,086	775	507	721	1,112	789	550
Underlying nightside FAC ($B_{U\text{-}n}$, $B_{D\text{-}n}$; kA)	847	883	921	742	758	851	821	693
Maximum substorm dayside FAC ($U_{S\text{-}d}$, $D_{S\text{-}d}$; kA)	135	154	134	69	145	150	157	90
Maximum substorm nightside FAC ($U_{S\text{-}n}$, $D_{S\text{-}n}$; kA)	291	289	298	345	288	274	294	330
Maximum total substorm FAC (ΣU_S, ΣD_S; kA)	410	440	430	403	410	417	446	398

Note. FACs are in kA; asymmetries are given as a ratio. Symbols and subscripts are defined in section 3.1.

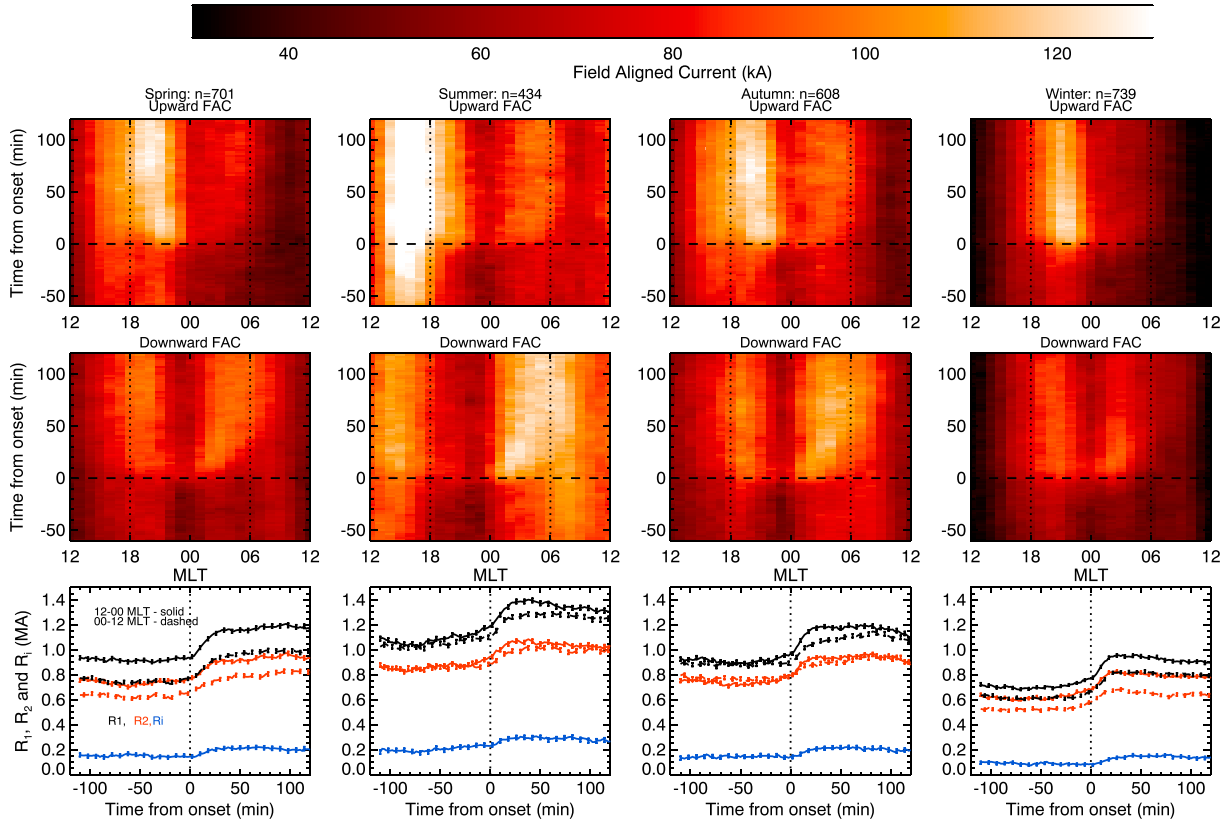

Figure 2. Superposed epoch analysis results with respect to substorm onset of the FACs from AMPERE. The top and middle rows show the integrated upward and downward FACs, respectively, in each MLT sector. The bottom row shows R_1 (black), R_2 (red), and R_i (blue) on the duskside (12–00 MLT; solid lines) and the dawnside (00–12 MLT; dashed lines). The results are subdivided into seasons, with each season defined as 90 days centered on the solstices or equinoxes. The error bars show the standard error in the means.

The Northern Hemisphere FACs show a dawn-dusk asymmetry that persists throughout the examined interval but that changes with season. This is evident in Figure 2 and summarized in Table 1. During winter and spring, R_1 and R_2 are 13–20% larger on the duskside than on the dawnside, $R_{2\text{-}pm}$ matching $R_{1\text{-}am}$. This dawn-dusk asymmetry is reduced to less than 5% in the summer and autumn. The ionospheric current R_i is small compared to R_1 and R_2, making up 20–24% of the R_1 current during the summer and 15–18% in the winter. The increase in ionospheric conductivity during the summer means that the polar cap potential, imposed by magnetospheric convection, drives larger ionospheric currents in the polar cap which must, in turn, be fed by large R_1 currents. It is interesting to note that the polar cap potential also shows a seasonal variation, peaking around the equinoxes rather than the solstices (de la Beaujardiere et al., 1991; Pettigrew et al., 2010; Ruohoniemi & Greenwald, 2005; Weimer, 1995; Zhang et al., 2007). This implies that the seasonal variation in ionospheric conductivity dominates the variations in the polar cap currents.

Following substorm onset, there is a marked increase in the nightside FACs, as expected with the appearance of the substorm current wedge. However, seasonal differences in the underlying currents (B_U and B_D) obscure changes to the FACs resulting from substorm activity. Figure 3 shows the upward and downward substorm FACs, S_U and S_D, and shows that after onset there is a marked increase in FACs, predominantly on the nightside. The FACs increase first near 00 MLT, subsequently expanding eastward and westward. This follows the expected pattern of the substorm current wedge. Figure 3 also shows an increase in the dayside currents, with a greater increase in the postnoon sector than in the prenoon sector.

Classically, the substorm current wedge was considered to be a Region 1-type current system, with the cross-tail current diverted into the ionosphere on the dawnside and the return current appearing on the duskside (Mcpherron et al., 1973). More recently, it has been suggested that the large-scale structure of the substorm current wedge consists of both Region 1- and Region 2-type current systems, with the Region 2-type current

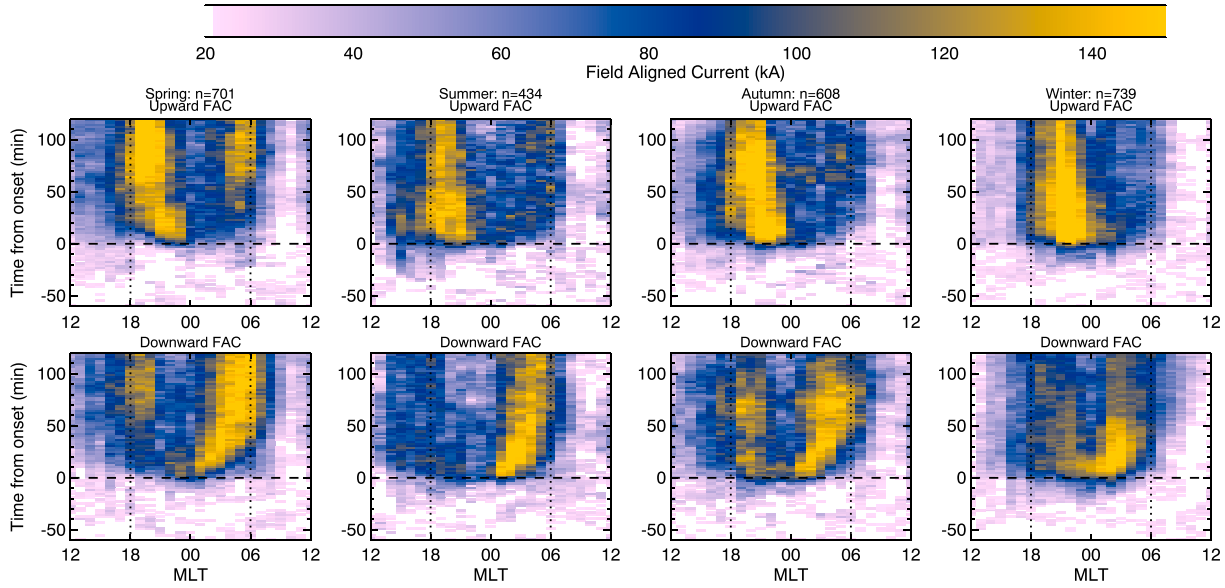

Figure 3. Superposed epoch analysis results with respect to substorm onset of the substorm FACs ($S_{U\text{-MLT}}$ and $S_{D\text{-MLT}}$) from AMPERE, calculated by removing the median current in the hour before onset. The top and bottom rows show the upward substorm FAC (S_U) and downward substorm FAC (S_D), respectively, in each MLT sector. As per the above, the results are subdivided into seasons of 90 days centered on the solstices and equinoxes.

system forming earthward of the Region 1-type system (Coxon et al., 2014a; Liu et al., 2016; Ritter & Luhr, 2008; Sergeev et al., 2011). Figure 3 shows that the nightside upward and downward FACs increase in both the premidnight and postmidnight sectors, with the upward current increasing more in the premidnight sector and the downward current increasing more in the postmidnight sector. As such, our results demonstrate enhancements in both Region 1-type and Region 2-type currents on the nightside, in keeping with these recent results.

Figure 3 shows that the substorm FACs are initially enhanced close to 00 MLT and then expand toward dawn and dusk. This is qualitatively in keeping with the expansion of the aurora (Milan et al., 2010). In general, the dawnward expansion of the FAC current is somewhat slower (~0.3 MLT/min) than the duskward expansion of the upward FAC (~0.7 MLT/min), as one might expect from the described morphology of substorm aurora including a westward traveling surge. Taking these to be speeds at a latitude of 65°, these correspond to a ground speed of 2 km/s for the eastward expanding downward current and 4 km/s for the westward expanding upward current. It is also interesting to note that the FACs near midnight rapidly decrease after they reach their peak to effectively give two separate regions of FAC enhancement. Given that the auroral and FAC features in this region can be complex and highly structured (Forsyth et al., 2014; Hoffman et al., 1994), AMPERE may not be able to resolve the FACs in this region; thus, further investigation is required to determine the extent to which FACs appear as small-scale and large-scale currents during substorms.

Summing S_U and S_D over 18–06 MLT, we find that the nightside currents increase by 290 kA in the first hour after onset in the spring, summer, and autumn. During the winter, the nightside currents increase by345 kA in the first hour after onset. The larger increase in the nightside currents during winter is offset by a smaller increase in the dayside currents. Overall, the FACs increase by an average of 420 kA in the hour after onset (Table 1). Figure 3 shows that the structure of these FACs varies subtly with season. In the winter, FACs are more concentrated on the nightside, resulting in higher FACs in individual MLT sectors. In the summer, the FAC is distributed over a greater range of MLT sectors resulting in smaller FAC peaks. We note that the dayside FACs during the summer are approximately double those during the winter (Table 1).

In summary, the Northern Hemisphere FACs during substorm vary seasonally, but this variation is dominated by changes in the underlying FAC system. If this variation is removed, we find that the FACs flowing as a result of substorm activity only vary by a small amount (~10%) with season. As such, the apparent seasonal variation in substorm FACs is the result of the superposition of an almost seasonally unvarying substorm current system and a seasonally varying underlying current system. The local time distribution of this substorm

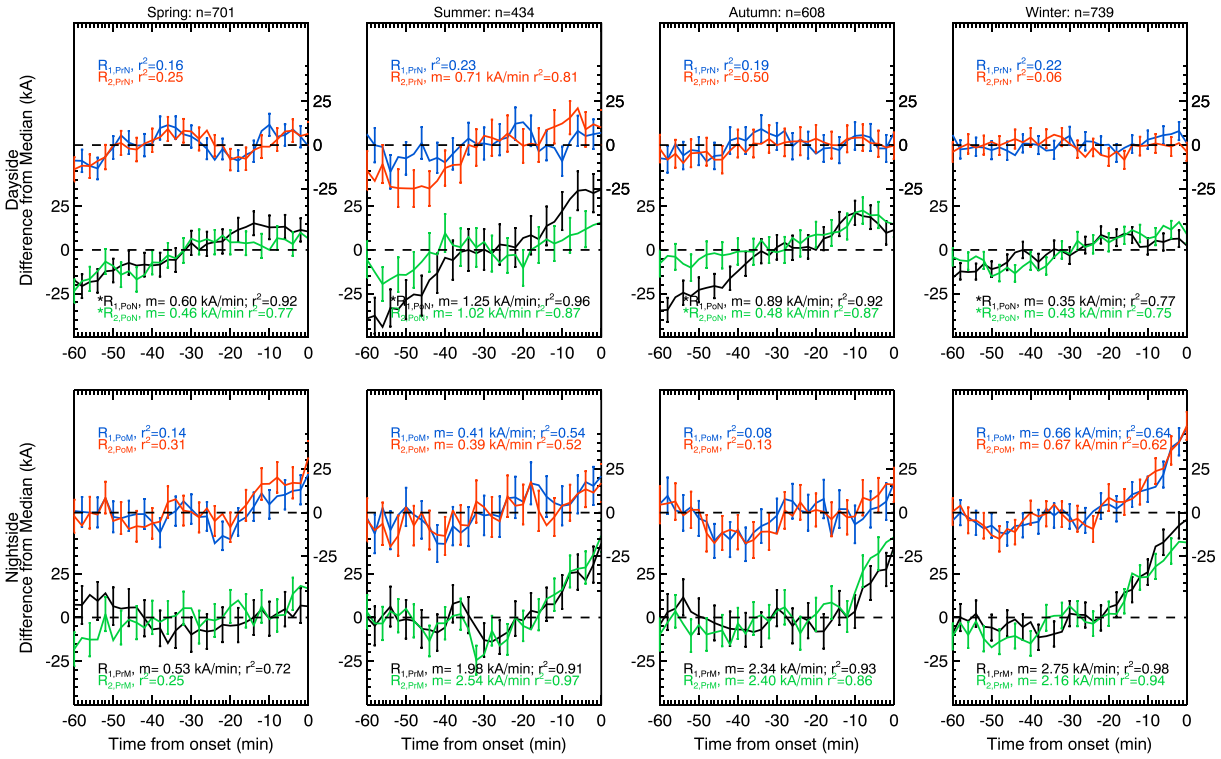

Figure 4. Superposed epoch analysis results of the dayside (top row) and nightside (bottom row) R_1 and R_2 FACs. In the top row, $R_{1,PrN}$ is in blue, $R_{1,PoN}$ is in black, $R_{2,PrN}$ is in red, and $R_{2,PoN}$ is in green. Similarly, on the bottom row $R_{1,PoM}$ is in blue, $R_{1,PrM}$ is in black, $R_{2,PoM}$ is in red, and $R_{2,PrM}$ is in green. As such, the dawnside FACs are in red and blue and the duskside FACs are in black and green. The FACs are shown for the hour leading up to onset and have had the median in that hour removed. As per the above, the results are subdivided into seasons of 90 days centered on the solstices and equinoxes. The error bars show the standard error in the mean. The linear correlation (r) and linear fit gradient (m) between each FAC and epoch are shown for each line. For the dayside and postmidnight FACs, this is calculated over the whole hour, whereas for the premidnight FACs, this is calculated for the 20 min prior to onset.

FAC changes subtly with season, with the substorm current being more concentrated on the nightside during the winter. It should be noted that the seasonal variations in FACs in the Southern Hemisphere may not match those of the Northern Hemisphere, and thus, the seasonal variability of the Southern Hemisphere component is needed to obtain a full picture of the global dynamics of FACs.

3.3. Variations in FACs Before Substorm Onset

In the growth phase prior to substorm onset, the magnetosphere goes through a period of gradual reconfiguration. Reconnection on the dayside opens up magnetic flux and adds magnetic energy into the system. The influence of dayside reconnection on polar cap convection propagates from the dayside toward the nightside over a period of ~15–20 min (Cowley & Lockwood, 1992). We expect this enhancement in convection to be accompanied by an enhancement in the FACs. Here we examine the temporal variation in FACs prior to substorm onset.

Figure 4 shows the results of a superposed epoch analysis of the Region 1 and Region 2 currents over the hour before onset in the prenoon and postnoon quadrants (top row) and premidnight and postmidnight quadrants (bottom row). As per Figures 2 and 3, the data are divided into spring, summer, autumn, and winter periods. The median current over the hour before onset in each quadrant has been removed.

There is a distinct dawn-dusk asymmetry in the variation of the dayside FACs prior to onset. $R_{1,PrN}$ and $R_{2,PrN}$ show little or no increase prior to onset, and the variations in the FACs show no linear correlation with time over 75%, with the exception of the $R_{2,PrN}$ currents in the summer. This increase in $R_{2,PrN}$ during the summer may be accounted for by considering that the Region 1 and Region 2 currents are not strictly split by the noon meridian; thus, this apparent increase may be a spillover from the mostly duskside FACs. In contrast, $R_{1,PoN}$ and $R_{2,PoN}$ show a linear increase of between 0.35 and 1.25 kA/min over the hour before onset, with a

correlation of 75–96%. In spring, summer, and autumn, $R_{1,PoN}$ increases faster than $R_{2,PoN}$, with the fastest rates of increase (1–1.25 kA/min) in the summer.

The variation in the nightside currents differs from the dayside FACs but retains a dawn-dusk asymmetry. In general, the premidnight FACs remain approximately constant until 20 min before onset, after which time they increase. This pattern is seen in the $R_{1,PrM}$ and $R_{2,PrM}$ in the summer, autumn, and winter and in $R_{1,PoM}$ and $R_{2,PoM}$ currents in the spring. The summer and winter $R_{1,PoM}$ and $R_{2,PoM}$ currents show a steady, albeit weakly correlated, increase throughout the hour before onset, in keeping with the dayside currents. The correlation between epoch and $R_{1,PoM}$ and $R_{2,PoM}$, respectively, does not exceed 65% and only exceed 60% in the winter; thus, the linearly fitted rates of increase of these FACs are not robust. The rates of increase of the well–correlated nightside FACs are all similar, with a mean value of 2.3 kA/min, which is significantly faster than the growth of the dayside currents.

Unlike the symmetric increase that one might expect in response to an increase in convection (e.g., Cowley & Lockwood, 1992), our observations show that most of the increase in FAC occurs on the duskside. The currents in the postnoon quadrant increase steadily over the hour prior to onset, whereas the currents in the prenoon MLT quadrant show no apparent variation. Furthermore, although the nightside currents also show an increase in FACs before substorm onset, the increase in these currents is delayed from the increase on the dayside and the rate of increase is notably faster, suggesting that the source of the current variations on the dayside and nightside is different. It is unclear why there is a dawn-dusk and day-night asymmetry in the variation of the current system. The dawn-dusk asymmetry has the opposite sense to the asymmetry in ionospheric conductivity associated with auroral precipitation (e.g., Hardy et al., 1987). As such, these results suggest that the driver of these currents varies not only from dayside to nightside, as indicated by the higher rates of increase on the nightside, but also in local time.

In general, the increases in the R_1 and R_2 currents in a given quadrant are similar and, as such, there is no significant increase in the polar cap or electrojet currents. This also implies that the Pedersen current crossing the auroral oval increases locally, that is, within each quadrant, prior to onset. Furthermore, the different rates and timings of increases in the dayside and nightside currents imply that these current systems are decoupled from one another. As such, while the net R_1 and R_2 currents increase prior to onset, this should not be considered a "global" increase.

3.4. Variations in FACs After Substorm Onset

The temporal profile of the ground magnetic perturbation due to substorms has previously been modeled using a simple capacitive-resistive circuit (Weimer, 1994):

$$J = J_1 + J_0 t e^{pt}$$

where J is the parameter of interest, t is time, p is a time constant, J_0 is an amplitude constant, and J_1 is an offset constant. This simple model was found to give a good fit to the averaged *AE* profile of substorms and the suggestion that the field-aligned currents should follow the same profile. Using data from AMPERE, we directly compare the observed FACs to this model.

The top row of Figure 5 shows the results of superposed epoch analysis of the R_1 (red), R_2 (green), and R_i currents (blue).The middle row shows the maximum of I_1, I_2, and I_i between 22 and 03 MLT for each time step, in the same way that the SuperMAG (SML) index shows the maximum negative magnetic field deflection. We define these as $I_{1\text{-max}}$, $I_{2\text{-max}}$, and $I_{i\text{-max}}$, respectively. The bottom row shows the results of superposed epoch analysis of the SuperMAG *AL* (SML). The overlaid dashed lines show the best fit of the Weimer (1994) function to data in the hour following substorm onset, obtained using the MPFIT procedure (Markwardt, 2009). We only fit this hour since the FACs and SML show a clear departure from this simple model after 1 hr, most likely due to the occurrence of further substorm activity. The best fit values for this function for all three currents and the SML magnetic indices are given in Table 2.

The top panels in Figure 5 show that R_1 and R_2 increase by up to 260 kA and 180 kA, respectively, in the hour after onset in each season. R_1 increases more than R_2 current; thus, there is an enhancement in R_i, the current flowing across the polar cap or through the auroral electrojets. This change in R_1 and R_2 after onset is different from that prior to onset, when they increase by similar amounts resulting in no increase in R_i. The global currents rapidly increase following substorm onset then remain elevated for most of the following 2 hr. In

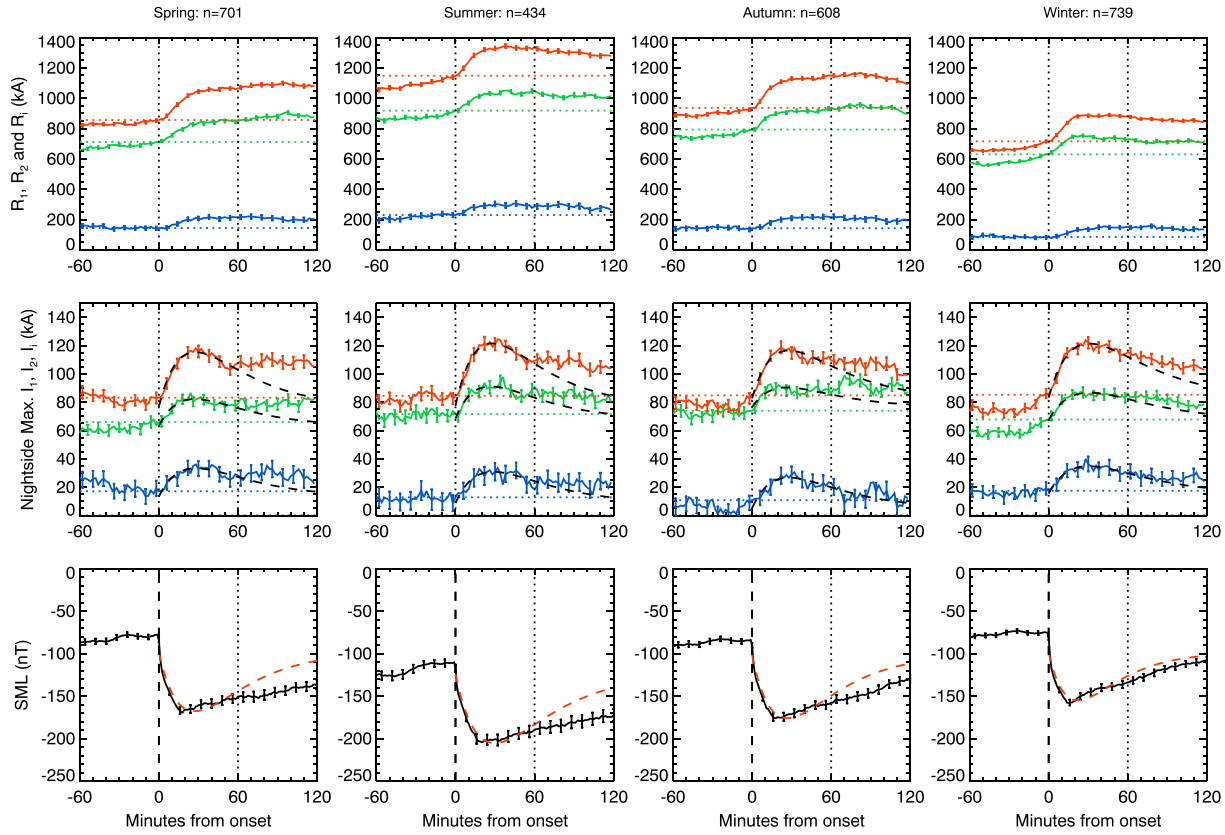

Figure 5. Superposed epoch analysis results with respect to substorm onset of (top row) R_1 (red), R_2 (green), and R_i (blue); (middle row) the maximum at each time step of I_1 (red), I_2 (green), and I_i (blue) between 22 and 03 MLT currents; and (bottom row) the SuperMAG *AL* (SML) index. In the middle and bottom rows, the dashed lines show the best fit results of the function $A_1 + A_0$ t exp(pt) (Weimer, 1994) to the data in the hour after onset, where t is time from onset and A_1, A_0, and p are constants. As per the above, the results are subdivided into seasons of 90 days centered on the solstices and equinoxes. The error bars show standard errors in the mean.

contrast, the nightside currents (middle row) and SML index (bottom row) reach a peak or trough ~20 min after onset before decaying back toward their initial values.

The dashed lines in Figure 5 show the best fit of the Weimer (1994) function to the nightside FACs and SML. The parameters of these best fits are given in Table 2. Over the hour following substorm onset, this model gives a good fit to the data, with correlations of 64–97%. Table 2 shows that the time constants (p) for the FACs and SML are similar, with a mean value of $-6 \times 10^{-4} \pm 0.13 \times 10^{-4}$/s. The time constants calculated for the winter FACs are systematically larger than all other seasons, whereas the time constant for the winter SML is smaller than all other seasons, although in both cases the time constants are within 3σ of the mean. This indicates that there is no seasonal variation in the time profile of the substorm FACs. Our results agree with the time constants determined by Weimer (1994) (-5×10^{-4} to -6.7×10^{-4}/s when converted into the same units), who did not separate their results by season.

Table 2
Values of the Best Fit Weimer (1994) Function for the $I_{1\text{-max}}$, $I_{2\text{-max}}$, $I_{i\text{-max}}$, and SML

	Spring	Summer	Autumn	Winter
$I_{1\text{-max}}$ J_1 (kA)	76	77	83	83
$I_{2\text{-max}}$ J_1 (kA)	63	68	76	68
$I_{i\text{-max}}$ J_1 (kA)	17	3	12	15
SML J_1 (nT)	−98	−125	−101	−99
$I_{1\text{-max}}$ J_0 (kA)	0.063	0.072	0.054	0.056
$I_{2\text{-max}}$ J_0 (kA)	0.032	0.038	0.024	0.28
$I_{i\text{-max}}$ J_0 (kA)	0.022	0.034	0.040	0.029
SML J_0 (nT)	0.12	0.12	0.13	0.12
$I_{1\text{-max}}$ p (s^{-1})	−6.0E−04	−6.0E−04	−6.0E−04	−5.4E−04
$I_{2\text{-max}}$ p (s^{-1})	−6.1E−04	−6.2E−04	−6.2E−04	−5.3E−04
$I_{i\text{-max}}$ p (s^{-1})	−4.7E−04	−6.6E−04	−5.7E−04	−5.5E−04
SML p (s^{-1})	−6.2E−04	−5.6E−04	−6.3E−04	−7.5E−04

During the hour after onset, the average SML decreases by ~85 nT. If we assume that the change in SML is due to a line current flowing at 100 km altitude, then this magnetic deflection requires a westward current of 42.5 kA. The average change in the nonlocally closed current after onset is~23 kA, half that required for the observed SML deflection.

In summary, our results show that both the Weimer (1994) functions provide a good fit to the nightside Region 1 and Region 2 FACs, as

well as the SML index, over the hour after substorm onset. Furthermore, the time constants of this function are in agreement and do not vary with season, showing that the temporal profile of the substorm current system does not vary with season. By examining the nonlocally closed currents on the nightside, we find that these currents are sufficient to account for half of the ground magnetic field deflection, if these currents are assumed to flow through the auroral electrojet.

4. Discussion

Using data from AMPERE and SuperMAG, we have examined the variations in field-aligned currents at all local times with respect to substorm onset and how these currents vary with Northern Hemisphere season. Our results show that the substorm current system is largely unchanged with season, increasing the overall current flowing by 420 kA through enhanced Region 1 and Region 2 currents on the nightside. The overall current system does vary with season; however, this is largely due to changes in the underlying currents, with the substorm FACs only varying by 10% between summer and winter. By examining the FACs determined in situ, we show that the substorm currents follow the Weimer (1994) model and have the same time constants as the ground magnetic field perturbations. Our results also show that the FACs increase prior to substorm onset. However, the dayside and nightside currents increase at different times before substorm onset; the postnoon currents increase linearly during the hour leading up to substorm onset, whereas the nightside currents are constant until 20–30 min before onset before increasing at nearly twice the rate of the dayside currents. Furthermore, there is a distinct dawn-dusk asymmetry in the increase of the FACs before onset, with the increase primarily found on the duskside.

4.1. Current System Asymmetries

Dawn-dusk asymmetries from different sources are prevalent throughout the solar wind-magnetosphere-ionosphere system (for a review, see Haaland et al., 2017, and Walsh et al., 2014). Our results demonstrate an asymmetry in the underlying FACs, namely, that can be as much as 20% stronger on the duskside. This asymmetry is strongest in the autumn and spring and can drop to as low as only 5% stronger on the duskside in the summer. Furthermore, our results show that prior to onset, the increase in FACs is concentrated on the duskside. The asymmetries observed in the total FACs derived from AMPERE in this study are different from the asymmetries in the current density from CHAMP reported by Huang et al. (2017), with the current densities in the Region 2 currents being up to 40% stronger at dawn. As noted in section 2, AMPERE predominantly detects large-scale currents, whereas single-spacecraft measurements of FACs can detect much smaller current systems; thus, these differences may arise from the underlying FAC calculations. However, the area through which the current is flowing also has to be accounted for and may account for the apparent difference between the Region 1 and Region 2 currents and current densities.

While this dawn-dusk asymmetry can be seen in the results of previous studies (e.g., Le et al., 2010), it has not been widely discussed in the literature. Nakano and Iyemori (2003) inferred an asymmetry in the Region 1 and Region 2 currents by examining the net upward and downward FACs from Dynamics Explorer 1. However, they were unable to determine which of the Region 1 or Region 2 currents was asymmetric. Our results show that both can be asymmetric and that this asymmetry will vary with season. However, in general, Region 1 is more asymmetric than Region 2. This asymmetry is in keeping with the dawn-dusk asymmetry in the current densities seen on the magnetopause (Haaland & Gjerloev, 2013), through which the Region 1 current is thought to close, although these authors note that the variation in the magnetopause width means that the total current flowing is similar at both dawn and dusk.

The dawn-dusk asymmetry in the variation of the dayside and nightside FACs prior to substorm onset is intriguing and, to our knowledge, has not previously been reported. The implication of this result is that ionospheric convection or conductivity is increased on the duskside during the substorm growth phase, while convection on the dawnside remains approximately constant (see Freeman et al., 1990, for a discussion on the links between FAC, convection, and conductivity). Statistical studies of the preonset ionospheric flows have not reported any such asymmetry (Grocott et al., 2009, 2010), although this was not a key focus of these studies. Specific investigations into this potentially unbalanced convection pattern or conductivity enhancement would be of interest but is beyond the scope of this study.

4.2. Seasonal Variations

It has previously been shown that FACs flowing into a given hemisphere vary with season (Coxon et al., 2016; Fujii et al., 1981; Ohtani et al., 2005). The illumination of the polar region varies throughout the year and hence influences the ionospheric conductivity in this region. As expected, this variation is greatest in the dayside ionospheric conductivity (e.g., Moen & Brekke, 1993). Assuming similar drivers for the FACs in all seasons, ionospheric conductivity and FAC strength will vary in tandem. This is fully evident in our results shown in Figure 1; the FACs are largest during the summer, and the greatest seasonal variation can be seen in the changes in the dayside FACs. Wang et al. (2005) similarly showed that the current density into and out of the Southern Hemisphere varied with solar illuminated conductivity and thus showed a seasonal and local time dependence.

While the quiescent FACs show a seasonal variation, the FACs that result from substorm activity are largely unchanged. This is in contrast to the reported semiannual variability of geomagnetic activity, which peaks at the equinoxes and reaches minima near at the solstices (Cortie, 1912; Russell & Mcpherron, 1973), although recent results have shown that this pattern does not necessarily hold in each year (Tanskanen et al., 2017) and maybe strongly influenced by the IMF (Zhao & Zong, 2012). Our results show that in each season, substorms add 420 kA on average to the total FAC flowing through the Northern Hemisphere, predominantly on the nightside. Fitting the Weimer function to the FACs and SML, we find that the time constants are the same for all seasons.

Chua et al. (2004) examined substorm timescales using hemispheric power calculated from Polar Ultraviolet Imager data. In their study, they explicitly separated out the expansion and recovery phases of substorms, calculating mean *e*-folding times for the recovery phase to be 35 min in the winter and 25 min in the summer. These times cannot be directly compared with the time constants determined in this study due to the assumed underlying form of the variation (e^{-pt} and te^{-pt} for the Chua et al. study and this study, respectively) and that the auroral luminosity and FACs are not linearly related. However, we can estimate the *e*-folding time by determining the time at which the Weimer (1994) function reaches e^{-1} of its maximum value. For the time constants determined in the Weimer (1994) study and in this study, the approximated *e*-folding time is 60 min, almost double that of Chua et al. (2004). Given that the particle energy flux from FACs is proportional to the square of the FAC (Cowley & Bunce, 2001), and taking auroral intensity to be proportional to this energy flux, the auroral *e*-folding time will be double that of the FACs. Thus, our timescales are similar to those of Chua et al. (2004) but do not show the same seasonal variation.

Tanskanen et al. (2011) and Mursula et al. (2011) both studied the seasonal variability of substorm occurrence, amplitude, and duration based on ground-based magnetometer data from the International Monitor for Auroral Geomagnetic Effects (IMAGE) network. They found the opposite seasonal variation of substorm duration to Chua et al. (2004), with longer substorms during the summer than during the winter. However, this is likely a result of their defining the end of a substorm as being when the IMAGE *AL* (IL) index reaches 20% of the minimum value in the substorm. Our results show that the baseline level of SML is 25%more negative during the summer than during the winter (Figure 4). As such, the change in SML required to reach the 20% of the minimum SML is greater during the summer than the winter, leading to longer substorms. If a similar annual variation in the baseline of the IL index is present, then this effect would be present in the Tanskanen et al. (2011) results. Furthermore, most substorm expansion phase onsets directly follow a recovery phase thus are compound events with multiple onsets (Forsyth et al., 2015). Each subsequent expansion phase onset will extend the apparent substorm duration, even though individual phases may be much shorter. Although Forsyth et al. (2015) did not examine the variation in substorm phase length with season, their average length of individual expansion and recovery phases combined was 1 hr, which is notably smaller than the 2.5–3.5 hr from Tanskanen et al. (2011).

From these previous studies, the extent to which substorms show seasonal variability is unclear. Our results show that the additional FACs from substorm activity and resulting ground magnetic deflections are largely unchanged with season. There is no seasonal difference in time constants or amplitudes of the substorm currents and ground-based magnetic deflections based on the superposed epoch analysis of AMPERE FACs and SML (see Table 2). However, the underlying FACs, and thus the impact of substorm currents on magnetosphere-ionosphere coupling, do have a seasonal variation. Around the winter solstice, the substorm currents increase the hemispheric FACs by 30–40% and the substorm current wedge appears as a well-defined current system (Figure 1). Around the summer solstice, the substorm currents increase the

hemispheric FACs by 20–25%, and while the substorm currents are visible, they are less distinct from the existing currents. The upward currents, in particular, remain weaker than the dayside currents. Shore et al. (2017) similarly found that the equivalent currents of the DP1 (substorm) current system provide a stronger contribution to the variability in high-latitude magnetometer data during the winter than during the summer.

4.3. Changes in Nightside FAC Before Onset

By subdividing the Northern Hemisphere FACs into the prenoon, postnoon, premidnight, and postmidnight quadrants, we found that there are distinct differences in the evolution of the FACs between the dayside and the nightside. Increases on the dayside are concentrated in the postnoon sector and occur over the whole of the hour before onset. On the nightside, the FACs remain approximately constant until 20–30 min before onset and then increase steadily. The rate of increase on the nightside is faster than that in the postnoon sector by a factor of 3.5 on average. This would imply that the FACs in these quadrants are decoupled, with the dayside and nightside FACs being driven by different processes.

In considering the increase in the statistically averaged FACs before substorm onset, we must consider the calculation of the FACs and the identification of the substorm onset. The AMPERE technique requires data collected over 10 min in order to estimate the FACs. In this study, we have deliberately time-tagged the FAC data with the end of the 10 min interval over which the raw data were captured (after Anderson et al., 2014) so as to minimize any effects from postonset FACs influencing the preonset FAC calculations. As such, only an uncertainty in the substorm onset timing would result in postonset magnetic deflections being included in the calculation of preonset FACs. Forsyth et al. (2015) showed that the majority of onsets from SOPHIE were within 20 min of previously defined auroral onsets. However, we would expect the effect on average FACs from AMPERE to be limited since SOPHIE picks out times when the ground magnetic perturbation from the ionospheric currents (fed by FACs) is enhanced, which may not be coincident with the first brightening of the aurora used to define onset. Thus, we interpret the enhancement in the FACs before substorm onset as a real feature.

Previous studies have shown the occurrence of pseudobreakups prior to substorm onset. These are normally identified as a brightening of the aurora that does not expand in the way that substorm auroral features do. Kullen et al. (2009, 2010) showed that pseudobreakups have very little effect on global magnetic indices and that they tend to occur for high-latitude substorms that tend to be weaker (Milan et al., 2009). While the occurrence of pseudobreakups may result in an increase in FACs before onset, from the above results we suggest that the impact that they would have on the average FACs calculated from AMPERE would be limited.

The growth of the nightside FACs in the 20–30 min prior to onset may indicate enhanced nightside coupling prior to substorm onset. The Vasyliunas (1970) equation describes the FAC from the plasma sheet to the ionosphere as the cross product of the pressure gradient and flux tube volume gradient or alternatively the dot product of the cross-tail current density and the flux tube volume gradient. Given that the flux tube volume decreases toward the Earth and that pressure is maximized along the central meridian of the magnetotail, this naturally describes a Region 2-type current system (e.g., Haerendel, 1990). As the current sheet thins during the growth phase (Hones et al., 1984; Mcpherron et al., 1973), the FACs will increase if the rate of change of the flux tube volume is smaller than the increase in the cross-tail current. A rapid increase in the cross-tail current density has been reported in case studies by Petrukovich et al. (2007) and Sergeev et al. (2011), with the latter showing that the current increased rapidly over the 15 min before onset, which is only slightly shorter than the timescale we observe for the average picture. However, our observations show that both the nightside Region 1 and Region 2 currents increase just prior to onset and the Vasyliunas (1970) can only explain the increase in a Region 1-type current if the gradients above are reversed or there is a strong inward pressure gradient. Such as pressure gradient has previously been postulated by Haerendel (2007). Thus, detailed observations of the azimuthal and radial pressure gradients and flux tube volume gradients are necessary to determine the extent to which variations in the magnetotail are linked to variations in the field-aligned currents.

An alternative explanation for the increase in nightside FACs prior to onset comes from examining changes in the ionosphere. Milan et al. (2010) showed that there is preexisting auroral brightness in the onset sector for up to an hour before substorm onset. This will naturally result in a local increase in conductivity. In turn, the

FACs will increase with conductivity so long as there is a constant electromotive force present. As the current increases, the electron precipitation into the ionosphere will also increase, possibly leading to positive feedback and further increase in conductivity and current, as first described by Atkinson (1970). This can create the so-called ionospheric feedback instability (Lysak,1991; Lysak & Song, 2002; Streltsov & Lotko, 2004, 2008; Sato, 1978; Trakhtengerts & Feldstein, 1991). This instability can disrupt the Pedersen currents associated with the large-scale downward current (Streltsov et al., 2010), possibly leading to the conditions for substorms onset. As such, the preonset currents and their interaction with the ionosphere may play a key role in determining the onset timing and location. However, the limitations of the FAC calculation by AMPERE, in particular the need to build up observations over 10 min and the lack of sensitivity to current densities below 0.2 μAm^2, mean that confirming this idea is difficult.

Recent studies have linked the phenomenon of aurora dimming (Pellinen & Heikkila, 1978) prior to substorm onset to decreases in the FACs as measured by AMPERE (Coxon et al., 2017; Murphy et al., 2012). Such a signature is not apparent in this statistical study. This is due to the relatively large area over which we sum the current observations. Murphy et al. (2012) and Coxon et al. (2017) showed that the reduction in the FACs prior to onset is limited to a localized area close to the onset region and not observed across the entire nightside. Our results show that on a more global scale, the FACs, on average, increase prior to onset.

4.4. Time Profiles of Postonset FACs

The simple model developed by Weimer (1994) assumes that the magnetosphere-ionosphere system can be described as an RC (resistor-capacitor) circuit. Furthermore, it assumes that the ground magnetic field perturbation is directly linked to the FACs. Given that the ground magnetic perturbation arises from Hall currents and that the ratio of ionospheric Hall and Pedersen conductivities varies with time and location during substorms (e.g., Gjerloev & Hoffman, 2000; Lester et al., 1996), it is not clear that the ground magnetic signature is representative of the FACs. In this study, we have directly compared the FACs with the Weimer model and found that both the FACs and the ground magnetic perturbations are well described by this model. Furthermore, the time constants for both the FACs and SML were ~6×10^{-4}/s, similar to the 4–6.5 $\times 10^{-4}$/s found by Weimer. This therefore implies that on a large statistical scale, the Weimer model holds.

Although our observations show that the FACs and ground magnetic perturbations show similar temporal profiles, a simple calculation of the nonlocally closed nightside current (i.e., the current that flows through the auroral electrojets) gives insufficient current to provide the observed ground magnetic field perturbation. The additional ground magnetic field perturbation may come about through small-scale up-down current pairs within MLT sectors that are not resolved by AMPERE. It has been proposed that the substorm current wedge could arise from the summation of a series of elemental currents (Birn & Hesse, 2013; Liu et al., 2015; Lyons et al., 2012, 2013; Rostoker, 1991; Zhang et al., 2011), which may or may not be linked to magnetospheric flows. Forsyth et al. (2014) showed that a large-scale substorm current wedge covering 4 hr of MLT had a longitudinal structure consisting of more than thirty ~100 km wide north-south aligned current sheets. These currents would close locally within each local time sector thus would not appear as a nonlocally closed current in our calculation, but their ionospheric closure currents could add to the overall ground magnetic perturbation. While AMPERE may not resolve these currents, our analysis shows that the classic large-scale structure of the substorm current wedge can be resolved and studied.

5. Conclusions

We have examined the seasonal variability of the substorm field-aligned current system along with how this current system varies before and after substorm onset using the AMPERE data set. Our results show the following:

1. Seasonal changes to the underlying system, predominantly on the dayside, dominate the overall variation in the substorm current systems. The current system resulting from the substorm activity is largely the same in each season.
2. There is a dawn-dusk asymmetry in the Region 1 and Region 2 current systems that is minimized during the summer and autumn and maximized in the winter and spring and that differs from the previously reported asymmetry in the Region 1 and Region 2 current densities.

3. FACs increase before substorm onset. There are linear increases on the dayside and nightside during the hour before onset and 20 min before onset, respectively. These increases are largely concentrated on the dusk side, with the dawnside currents showing little or no preonset increase.
4. Nightside FACs and the SML index follow the Weimer (1994) model, with time constants that are similar in all seasons. The FACs that are not locally closed on the nightside are sufficiently strong to account for half of the magnetic perturbation observed on the ground.

Acknowledgments
AMPERE data are available to download at ampere.jhuapl.edu. The substorm onsets from SOPHIE are included in the Supplementary Information of Forsyth et al. (2015). OMNI solar wind data are available from cdaweb.gsfc.nasa.gov. SuperMAG SML and SMU data are available from supermag.jhuapl.edu. We thank the AMPERE team and the AMPERE Science Center for providing the Iridium derived data products. For the ground magnetometer data we gratefully acknowledge the following: Intermagnet; USGS, Jeffrey J. Love; CARISMA, PI Ian Mann; CANMOS; the S-RAMP Database, PI K. Yumoto and Dr. K. Shiokawa; the SPIDR database; AARI, PI Oleg Troshichev; the MACCS program, PI M. Engebretson, Geomagnetism Unit of the Geological Survey of Canada; GIMA; MEASURE, UCLA IGPP, and Florida Institute of Technology; SAMBA, PI Eftyhia Zesta; 210 Chain, PI K. Yumoto; SAMNET, PI Farideh Honary; the institutes who maintain the IMAGE magnetometer array, PI Eija Tanskanen; PENGUIN; AUTUMN, PI Martin Connors; DTU Space, PI Dr. Juergen Matzka; South Pole and McMurdo Magnetometer, PIs Louis J. Lanzarotti and Alan T. Weatherwax; ICESTAR; RAPIDMAG; PENGUIn; British Antarctic Survey; McMac, PI Dr. Peter Chi; BGS, PI Dr. Susan Macmillan; Pushkov Institute of Terrestrial Magnetism, Ionosphere and Radio Wave Propagation (IZMIRAN); GFZ, PI Dr. Juergen Matzka; MFGI, PI B. Heilig; IGFPAS, PI J. Reda; University of L'Aquila, PI M. Vellante; and SuperMAG, PI Jesper W. Gjerloev. C. F. and I. J. R. are funded in part by Natural Environment Research Council (NERC) grants NE/L007495/1 and NE/M00886X/1. C. F. is also funded by NERC IRF NE/N014480/1. I. J. R. and N. M. E. K. are funded by Science and Technology Facilities Council (STFC), UK, grant ST/N000722/1. C. M. J. and J. C. C. are funded by NERC grant NE/L007177/1. C. M. J. is also supported by an STFC Ernest Rutherford Fellowship, and J. C. C. is also funded by STFC grant ST/L002809/1. M. P. F.'s contribution is funded by NERC grant NE/L006456/1. S. E. M. was supported by the Science and Technology Facilities Council (STFC), UK, grant ST/N000749/1. Support for AMPERE has been provided under NSF sponsorship under grants ATM-0739864 and AGS-1420184.

References

Akasofu, S.-I., & Chapman, S. (1972). *Solar-terrestrial physics: An account of the wave and particle radiations from the quiet and the active sun, and of the consequent terrestrial phenomena, The International Series of Monographs on Physics*. Oxford: Clarendon Press.

Anderson, B. J., Korth, H., Waters, C. L., Green, D. L., Merkin, V. G., Barnes, R. J., & Dyrud, L. P. (2014). Development of large-scale Birkeland currents determined from the Active Magnetosphere And Planetary Electrodynamics Response Experiment. *Geophysical Research Letters*, *41*, 3017–3025. https://doi.org/10.1002/2014GL059941

Anderson, B. J., Korth, R., Waters, C. L., Green, D. L., & Stauning, P. (2008). Statistical Birkeland current distributions from magnetic field observations by the Iridium constellation. *Annales Geophysicae-Germany*, *26*(3), 671–687. https://doi.org/10.5194/angeo-26-671-2008

Anderson, B. J., Takahashi, K., Kamei, T., Waters, C. L., & Toth, B. A. (2002). Birkeland current system key parameters derived from Iridium observations: Method and initial validation results. *Journal of Geophysical Research*, *107*(A6), 1079. https://doi.org/10.1029/2001JA000080

Anderson, B. J., Takahashi, K., & Toth, B. A. (2000). Sensing global Birkeland currents with Iridium(R) engineering magnetometer data. *Geophysical Research Letters*, *27*(24), 4045–4048. https://doi.org/10.1029/2000GL000094

Atkinson, G. (1970). Auroral arcs—Result of interaction of a dynamic magnetosphere with ionosphere. *Journal of Geophysical Research*, *75*(25), 4746–4755. https://doi.org/10.1029/JA075i025p04746

Birn, J., & Hesse, M. (2013). The substorm current wedge in MHD simulations. *Journal of Geophysical Research Space Physics*, *118*, 3364–3376. https://doi.org/10.1002/jgra.50187

Chua, D., Parks, G., Brittnacher, M., Germany, G., & Spann, J. (2004). Auroral substorm timescales: IMF and seasonal variations. *Journal of Geophysical Research*, *109*, A03207. https://doi.org/10.1029/2003JA009951

Clausen, L. B. N., Baker, J. B. H., Ruohoniemi, J. M., Milan, S. E., & Anderson, B. J. (2012). Dynamics of the region 1 Birkeland current oval derived from the Active Magnetosphere And Planetary Electrodynamics Response Experiment (AMPERE). *Journal of Geophysical Research*, *117*, A06233. https://doi.org/10.1029/2012JA017666

Clausen, L. B. N., Baker, J. B. H., Ruohoniemi, J. M., Milan, S. E., Coxon, J. C., Wing, S., et al. (2013). Temporal and spatial dynamics of the regions 1 and 2 Birkeland currents during substorms. *Journal of Geophysical Research: Space Physics*, *118*, 3007–3016. https://doi.org/10.1002/jgra.50288

Clausen, L. B. N., Milan, S. E., Baker, J. B. H., Ruohoniemi, J. M., Glassmeier, K. H., Coxon, J. C., & Anderson, B. J. (2013). On the influence of open magnetic flux on substorm intensity: Ground- and space-based observations. *Journal of Geophysical Research: Space Physics*, *118*, 2958–2969. https://doi.org/10.1002/jgra.50308

Cortie, A. L. (1912). Sun-spots and terrestrial magnetic phenomena, 1898-1911: The cause of the annual variation in magnetic disturbances. *Monthly Notices of the Royal Astronomical Society*, *73*(1), 52–0060. https://doi.org/10.1093/mnras/73.1.52

Cowley, S. W. (2000). Magnetosphere-Ionosphere Interactions: A Tutorial Review. In S. Ohtani, et al. (Eds.), *Magnetospheric current systems, Geophysical Monograph Series*. Washington, DC: American Geophysical Union. https://doi.org/10.1029/GM118p0091

Cowley, S. W. H., & Bunce, E. J. (2001). Origin of the main auroral oval in Jupiter's coupled magnetosphere–ionosphere system. *Planetary and Space Science*, *49*(10–11), 1067–1088. https://doi.org/10.1016/S0032-0633(00)00167-7

Cowley, S. W. H., & Lockwood, M. (1992). Excitation and decay of solar wind-driven flows in the magnetosphere-ionosphere system. *Annales Geophysicae*, *10*(1–2), 103–115.

Coxon, J. C., Milan, S. E., Carter, J. A., Clausen, L. B. N., Anderson, B. J., & Korth, H. (2016). Seasonal and diurnal variations in AMPERE observations of the Birkeland currents compared to modeled results. *Journal of Geophysical Research: Space Physics*, *121*, 4027–4040. https://doi.org/10.1002/2015JA022050

Coxon, J. C., Milan, S. E., Clausen, L. B. N., Anderson, B. J., & Korth, H. (2014a). The magnitudes of the regions 1 and 2 Birkeland currents observed by AMPERE and their role in solar wind-magnetosphere-ionosphere coupling. *Journal of Geophysical Research: Space Physics*, *119*, 9804–9815. https://doi.org/10.1002/2014JA020138

Coxon, J. C., Milan, S. E., Clausen, L. B. N., Anderson, B. J., & Korth, H. (2014b). A superposed epoch analysis of the regions 1 and 2 Birkeland currents observed by AMPERE during substorms. *Journal of Geophysical Research: Space Physics*, *119*, 9834–9846. https://doi.org/10.1002/2014JA020500

Coxon, J. C., Milan, S. E., & Anderson, B. J. (2018). A Review of Birkeland Current Research using AMPERE. In A. Keiling, O. Marghitu, & M. Wheatland (Eds.), *Electric currents in geospace and beyond* (Chap. 16). Washington, DC: American Geophysical Union. Retrieved from https://www.wiley.com/en-us/Electric+Currents+in+Geospace+and+Beyond-p-9781119324492. https://doi.org/10.1002/9781119324522.ch16

Coxon, J. C., Rae, I. J., Forsyth, C., Jackman, C. M., Fear, R. C., & Anderson, B. J. (2017). Birkeland currents during substorms: Statistical evidence for intensification of Regions 1 and 2 currents after onset and a localized signature of auroral dimming. *Journal of Geophysical Research: Space Physics*, *122*, 6455–6468. https://doi.org/10.1002/2017JA023967

de la Beaujardiere, O., Alcayde, D., Fontanari, J., & Leger, C. (1991). Seasonal dependence of high-latitude electric fields. *Journal of Geophysical Research*, *96*(A4), 5723–5735. https://doi.org/10.1029/90JA01987

Dunlop, M. W., Yang, Y. Y., Yang, J. Y., Lühr, H., Shen, C., Olsen, N., et al. (2015). Multispacecraft current estimates at swarm. *Journal of Geophysical Research: Space Physics*, *120*, 8307–8316. https://doi.org/10.1002/2015JA021707

Forsyth, C., Fazakerley, A. N., Rae, I. J., J. Watt, C. E., Murphy, K., Wild, J. A., et al. (2014). In situ spatiotemporal measurements of the detailed azimuthal substructure of the substorm current wedge. *Journal of Geophysical Research: Space Physics*, *119*, 927–946. https://doi.org/10.1002/2013JA019302

Forsyth, C., Rae, I. J., Coxon, J. C., Freeman, M. P., Jackman, C. M., Gjerloev, J., & Fazakerley, A. N. (2015). A new technique for determining Substorm Onsets And Phases From Indices of the Electrojet (SOPHIE). *Journal of Geophysical Research: Space Physics*, *120*, 10,592–10,606. https://doi.org/10.1002/2015JA021343

Forsyth, C., Rae, I. J., Mann, I. R., & Pakhotin, I. P. (2017). Identifying intervals of temporally invariant field-aligned currents from Swarm: Assessing the validity of single-spacecraft methods. *Journal of Geophysical Research: Space Physics*, *122*, 3411–3419. https://doi.org/10.1002/2016JA023708

Freeman, M. P., Southwood, D. J., Lester, M., & Waldock, J. A. (1990). Measurement of field-aligned currents by the sabre coherent scatter radar. In C. T. Russell, E. R. Priest, & L. C. Lee (Eds.), *Physics of magnetic flux ropes*. Washington, DC: American Geophysical Union. https://doi.org/10.1029/GM058p0575

Friedrich, E., & Rostoker, G. (1998). *Reconfiguration of the directly driven currents during a substorm expansive phase: Implications for the substormcurrent wedge*. Paper Presented at SUBSTORMS-4, Terra Sci. Publ. Co., Kluwer Acad. Publ., Tokyo.

Fujii, R., Iijima, T., Potemra, T. A., & Sugiura, M. (1981). Seasonal dependence of large-scale Birkeland currents. *Geophysical Research Letters*, *8*, 1103–1106. https://doi.org/10.1029/GL008i010p01103

Gjerloev, J. W. (2012). The SuperMAG data processing technique. *Journal of Geophysical Research*, *117*, A09213. https://doi.org/10.1029/2012JA017683

Gjerloev, J. W., & Hoffman, R. A. (2000). Height-integrated conductivity in auroral substorms: 2. Modeling. *Journal of Geophysical Research*, *105*(A1), 227–235. https://doi.org/10.1029/1999JA900353

Gjerloev, J. W., & Hoffman, R. A. (2002). Currents in auroral substorms. *Journal of Geophysical Research*, *107*(A8), 1163. https://doi.org/10.1029/2001JA000194

Gjerloev, J. W., Ohtani, S., Iijima, T., Anderson, B., Slavin, J., & Le, G. (2011). Characteristics of the terrestrial field-aligned current system. *Annales Geophysicae-Germany*, *29*(10), 1713–1729. https://doi.org/10.5194/angeo-29-1713-2011

Green, D. L., Waters, C. L., Anderson, B. J., Korth, H., & Barnes, R. J. (2006). Comparison of large-scale Birkeland currents determined from iridium and SuperDARN data. *Annales Geophysicae-Germany*, *24*(3), 941–959. https://doi.org/10.5194/angeo-24-941-2006

Grocott, A., Milan, S. E., Yeoman, T. K., Sato, N., Yukimatu, A. S., & Wild, J. A. (2010). Superposed epoch analysis of the ionospheric convection evolution during substorms: IMF BY dependence. *Journal of Geophysical Research*, *115*, A00I06. https://doi.org/10.1029/2010JA015728

Grocott, A., Wild, J. A., Milan, S. E., & Yeoman, T. K. (2009). Superposed epoch analysis of the ionospheric convection evolution during substorms: Onset latitude dependence. *Annales Geophysicae*, *27*, 591–600. https://doi.org/10.5194/angeo-27-591-2009

Haaland, S., & Gjerloev, J. (2013). On the relation between asymmetries in the ring current and magnetopause current. *Journal of Geophysical Research: Space Physics*, *118*, 7593–7604. https://doi.org/10.1002/2013JA019345

Haaland, S. E., Runov, A., & Forsyth, C. (Eds.) (2017). *Dawn-dusk asymmetries in planetary plasma environments*. Hoboken, NJ: John Wiley.

Haerendel, G. (1990). Field-aligned currents in the Earth's Magnetosphere. In C. T. Russell, E. R. Priest, & L. C. Lee (Eds.), *Physics of magnetic flux ropes*. Washington, DC: American Geophysical Union. https://doi.org/10.1029/GM058p0539

Haerendel, G. (2007). Auroral arcs as sites of magnetic stress release. *Journal of Geophysical Research*, *112*, A09214. https://doi.org/10.1029/2007JA012378

Hardy, D. A., Gussenhoven, M. S., Raistrick, R., & McNeil, W. J. (1987). Statistical and functional representations of the pattern of auroral energy flux, number flux, and conductivity. *Journal of Geophysical Research*, *92*(A11), 12,275–12,275. https://doi.org/10.1029/JA092iA11p12275

He, M. S., Vogt, J., Luhr, H., & Sorbalo, E. (2014). Local time resolved dynamics of field-aligned currents and their response to solar wind variability. *Journal of Geophysical Research: Space Physics*, *119*, 5305–5315. https://doi.org/10.1002/2014JA019776

Hoffman, R. A., Fujii, R., & Sugiura, M. (1994). Characteristics of the field-aligned current system in the nighttime sector during auroral substorms. *Journal of Geophysical Research*, *99*(A11), 21,303–21,325. https://doi.org/10.1029/94JA01659

Hones, E. W., Pytte, T., & West, H. I. (1984). Associations of geomagnetic-activity with plasma sheet thinning and expansion—A statistical study. *Journal of Geophysical Research*, *89*(A7), 5471–5478. https://doi.org/10.1029/JA089iA07p05471

Huang, T., Luhr, H., & Wang, H. (2017). Global characteristics of auroral Hall currents derived from the Swarm constellation: Dependences on season and IMF orientation. *Annales Geophysicae-Germany*, *35*(6), 1249–1268. https://doi.org/10.5194/angeo-35-1249-2017

Huang, T., Luhr, H., Wang, H., & Xiong, C. (2017). The relationship of high-latitude thermospheric wind with ionospheric horizontal current, as observed by CHAMP satellite. *Journal of Geophysical Research: Space Physics*, *122*, 12,378–12,392. https://doi.org/10.1002/2017JA024614

Iijima, T., & Potemra, T. A. (1976). Amplitude distribution of field-aligned currents at northern high latitudes observed by Triad. *Journal of Geophysical Research*, *81*(13), 2165–2174. https://doi.org/10.1029/JA081i013p02165

Iijima, T., & Potemra, T. A. (1978). Large-scale characteristics of field-aligned currents associated with substorms. *Journal of Geophysical Research*, *83*(A2), 599–615. https://doi.org/10.1029/JA083iA02p00599

Juusola, L., Kauristie, K., Amm, O., & Ritter, P. (2009). Statistical dependence of auroral ionospheric currents on solar wind and geomagnetic parameters from 5 years of CHAMP satellite data. *Annales Geophysicae-Germany*, *27*(3), 1005–1017. https://doi.org/10.5194/angeo-27-1005-2009

Juusola, L., Milan, S. E., Lester, M., Grocott, A., & Imber, S. M. (2014). Interplanetary magnetic field control of the ionospheric field-aligned current and convection distributions. *Journal of Geophysical Research: Space Physics*, *119*, 3130–3149. https://doi.org/10.1002/2013JA019455

Kamide, Y., Sun, W., & Akasofu, S.-I. (1996). The average ionospheric electrodynamics for the different substorm phases. *Journal of Geophysical Research*, *101*(A1), 99–109. https://doi.org/10.1029/95JA02990

Kepko, L., McPherron, R. L., Amm, O., Apatenkov, S., Baumjohann, W., Birn, J., et al. (2015). Substorm current wedge revisited. *Space Science Reviews*, *190*, 1–46. https://doi.org/10.1007/s11214-014-0124-9

Kullen, A., Karlsson, T., Cumnock, J. A., & Sundberg, T. (2010). Occurrence and properties of substorms associated with pseudobreakups. *Journal of Geophysical Research*, *115*, A12310. https://doi.org/10.1029/2010JA015866

Kullen, A., Ohtani, S., & Karlsson, T. (2009). Geomagnetic signatures of auroral substorms preceded by pseudobreakups. *Journal of Geophysical Research*, *114*, A04201. https://doi.org/10.1029/2008JA013712

Le, G., Slavin, J. A., & Strangeway, R. J. (2010). Space Technology 5 observations of the imbalance of regions 1 and 2 field-aligned currents and its implication to the cross-polar cap Pedersen currents. *Journal of Geophysical Research*, *115*, A07202. https://doi.org/10.1029/2009JA014979

Lester, M., Davies, J. A., & Virdi, T. S. (1996). High-latitude Hall and Pedersen conductances during substorm activity in the SUNDIAL-ATLAS campaign. *Journal of Geophysical Research*, *101*(A12), 26,719–26,728. https://doi.org/10.1029/96JA00979

Liu, J., Angelopoulos, V., Chu, X., & McPherron, R. L. (2016). Distribution of Region 1 and 2 currents in the quiet and substorm time plasma sheet from THEMIS observations. *Geophysical Research Letters*, *43*, 7813–7821. https://doi.org/10.1002/2016GL069475

Liu, J., Angelopoulos, V., Chu, X., Zhou, X., & Yue, C. (2015). Substorm current wedge composition by wedgelets. *Geophysical Research Letters*, *42*, 1669–1676. https://doi.org/10.1002/2015GL063289

Lühr, H., Park, J., Gjerloev, J. W., Rauberg, J., Michaelis, I., Merayo, J. M. G., & Brauer, P. (2015). Field-aligned currents' scale analysis performed with the Swarm constellation. *Geophysical Research Letters*, *42*, 1–8. https://doi.org/10.1002/2014GL062453

Lühr, H., Rother, M., Kohler, W., Ritter, P., & Grunwaldt, L. (2004). Thermospheric up-welling in the cusp region: Evidence from CHAMP observations. *Geophysical Research Letters*, *31*, L06805. https://doi.org/10.1029/2003GL019314

Lyons, L. R., Nishimura, Y., Donovan, E., & Angelopoulos, V. (2013). Distinction between auroral substorm onset and traditional ground magnetic onset signatures. *Journal of Geophysical Research Space Physics*, *118*, 4080–4092. https://doi.org/10.1002/jgra.50384

Lyons, L. R., Nishimura, Y., Xing, X., Runov, A., Angelopoulos, V., Donovan, E., & Kikuchi, T. (2012). Coupling of dipolarization front flow bursts to substorm expansion phase phenomena within the magnetosphere and ionosphere. *Journal of Geophysical Research*, *117*, A02212. https://doi.org/10.1029/2011JA017265

Lysak, R. L. (1991). Feedback instability of the ionospheric resonant cavity. *Journal of Geophysical Research*, *96*(A2), 1553–1568. https://doi.org/10.1029/90JA02154

Lysak, R. L., & Song, Y. (2002). Energetics of the ionospheric feedback interaction. *Journal of Geophysical Research*, *107*(A8), 1160. https://doi.org/10.1029/2001JA000308

Markwardt, C. B. (2009). "Non-Linear Least Squares Fitting in IDL with MPFIT." In D. Bohlender, P. Dowler, & D. Durand (Eds.), *Proc. Astronomical Data Analysis Software and Systems XVIII, Quebec, Canada, ASP Conference Series* (Vol. 411, pp. 251–254). San Francisco, CA: Astronomical Society of the Pacific.

McGranaghan, R. M., Mannucci, A. J., & Forsyth, C. (2017). A comprehensive analysis of multiscale field-aligned currents: Characteristics, controlling parameters, and relationships. *Journal of Geophysical Research: Space Physics*, *122*, 11,931–11,960. https://doi.org/10.1002/2017JA024742

Mcpherron, R. L., Russell, C. T., & Aubry, M. P. (1973). Satellite studies of magnetospheric substorms on August 15, 1968: 9. Phenomenological model for substorms. *Journal of Geophysical Research*, *78*(16), 3131–3149. https://doi.org/10.1029/JA078i016p03131

Milan, S. E., Carter, J. A., Korth, H., & Anderson, B. J. (2015). Principal component analysis of Birkeland currents determined by the Active Magnetosphere And Planetary Electrodynamics Response Experiment. *Journal of Geophysical Research: Space Physics*, *120*, 10,415–10,424. https://doi.org/10.1002/2015JA021680

Milan, S. E., Clausen, L. B. N., Coxon, J. C., Carter, J. A., Walach, M. T., Laundal, K., et al. (2017). Overview of solar Wind–Magnetosphere–Ionosphere–Atmosphere coupling and the generation of magnetospheric currents. *Space Science Reviews*, *206*, 547–573. https://doi.org/10.1007/s11214-017-0333-0

Milan, S. E., Grocott, A., Forsyth, C., Imber, S. M., Boakes, P. D., & Hubert, B. (2009). A superposed epoch analysis of auroral evolution during substorm growth, onset and recovery: Open magnetic flux control of substorm intensity. *Annales Geophysicae-Germany*, *27*(2), 659–668. https://doi.org/10.5194/angeo-27-659-2009

Milan, S. E., Grocott, A., & Hubert, B. (2010). A superposed epoch analysis of auroral evolution during substorms: Local time of onset region. *Journal of Geophysical Research*, *115*, A00I04. https://doi.org/10.1029/2010JA015663

Miles, D. M., Mann, I. R., Pakhotin, I. P., Burchill, J. K., Howarth, A. D., Knudsen, D. J., et al. (2018). Alfvénic dynamics and fine structuring of discrete auroral arcs: Swarm and e-POP observations. *Geophysical Research Letters*, *45*, 545–555. https://doi.org/10.1002/2017GL076051

Moen, J., & Brekke, A. (1993). The solar flux influence on quiet-time conductances in the auroral ionosphere. *Geophysical Research Letters*, *20*, 971–974.

Murphy, K. R., Mann, I. R., Rae, I. J., Waters, C. L., Anderson, B. J., Milling, D. K., et al. (2012). Reduction in field-aligned currents preceding and local to auroral substorm onset. *Geophysical Research Letters*, *39*, L15106. https://doi.org/10.1029/2012GL052798

Mursula, K., Tanskanen, E., & Love, J. J. (2011). Spring-fall asymmetry of substorm strength, geomagnetic activity and solar wind: Implications for semiannual variation and solar hemispheric asymmetry. *Geophysical Research Letters*, *38*, L06104. https://doi.org/10.1029/2011GL046751

Nakano, S., & Iyemori, T. (2003). Local time distribution of net field-aligned currents derived from high-altitude satellite data. *Journal of Geophysical Research*, *108*, 1314. https://doi.org/10.1029/2002JA009519

Neubert, T., & Christiansen, F. (2003). Small-scale, field-aligned currents at the top-side ionosphere. *Geophysical Research Letters*, *30*(19), 2010. https://doi.org/10.1029/2003GL017808

Newell, P. T., & Gjerloev, J. W. (2011). Evaluation of SuperMAG auroral electrojet indices as indicators of substorms and auroral power. *Journal of Geophysical Research*, *116*, A12211. https://doi.org/10.1029/2011JA016779

Ohtani, S., Ueno, G., Higuchi, T., & Kawano, H. (2005). Annual and semiannual variations of the location and intensity of large-scale field-aligned currents. *Journal of Geophysical Research*, *110*, A01216. https://doi.org/10.1029/2004JA010634

Pakhotin, I. P., Mann, I. R., Lysak, R. L., Knudsen, D. J., Gjerloev, J. W., Rae, I. J., et al. (2018). Diagnosing the role of Alfvén waves in magnetosphere-ionosphere coupling: Swarm observations of large amplitude nonstationary magnetic perturbations during an interval of northward IMF. *Journal of Geophysical Research: Space Physics*, *123*, 326–340. https://doi.org/10.1002/2017JA024713

Papitashvili, V. O., Christiansen, F., & Neubert, T. (2002). A new model of field-aligned currents derived from high-precision satellite magnetic field data. *Geophysical Research Letters*, *29*(14), 1683. https://doi.org/10.1029/2001GL014207

Pellinen, R. J., & Heikkila, W. J. (1978). Observations of auroral fading before breakup. *Journal of Geophysical Research*, *83*(A9), 4207–4217. https://doi.org/10.1029/JA083iA09p04207

Pettigrew, E. D., Shepherd, S. G., & Ruohoniemi, J. M. (2010). Climatological patterns of high-latitude convection in the Northern and Southern hemispheres: Dipole tilt dependencies and interhemispheric comparisons. *Journal of Geophysical Research*, *115*, A07305. https://doi.org/10.1029/2009JA014956

Petrukovich, A. A., Baumjohann, W., Nakamura, R., Runov, A., Balogh, A., & Reme, H. (2007). Thinning and stretching of the plasma sheet. *Journal of Geophysical Research*, *112*, A10213. https://doi.org/10.1029/2007JA012349

Ritter, P., & Luhr, H. (2008). Near-Earth magnetic signature of magnetospheric substorms and an improved substorm current model. *Annales Geophysicae-Germany*, *26*(9), 2781–2793. https://doi.org/10.5194/angeo-26-2781-2008

Rostoker, G. (1974). Current flow in magnetosphere during magnetospheric substorms. *Journal of Geophysical Research*, *79*(13), 1994–1998. https://doi.org/10.1029/JA079i013p01994

Rostoker, G. (1991). Some observational constraints for substorm models. In *Magnetospheric Substorms, Geophysical Monograph Series* (Vol. 64, pp. 61–72). Washington, DC: American Geophysical Union. https://doi.org/10.1029/GM064p0061

Rostoker, G., & Friedrich, E. (2005). Creation of the substorm current wedge through the perturbation of the directly driven current system: A new model for substorm expansion. *Annales Geophysicae-Germany*, *23*(6), 2171–2182. https://doi.org/10.5194/angeo-23-2171-2005

Rother, M., Schlegel, K., & Luhr, H. (2007). CHAMP observation of intense kilometer-scale field-aligned currents, evidence for an ionospheric Alfven resonator. *Annales Geophysicae-Germany*, *25*(7), 1603–1615. https://doi.org/10.5194/angeo-25-1603-2007

Ruohoniemi, J. M., & Greenwald, R. A. (2005). Dependencies of high-latitude plasma convection: Consideration of interplanetary magnetic field, seasonal, and universal time factors in statistical patterns. *Journal of Geophysical Research*, *110*, A09204. https://doi.org/10.1029/2004JA010815

Russell, C. T., & Mcpherron, R. L. (1973). Semiannual variation of geomagnetic activity. *Journal of Geophysical Research*, *78*(1), 92–108. https://doi.org/10.1029/JA078i001p00092

Sato, T. (1978). Nonlinear transport instability in a diffusive plasma. *Physics of Fluids*, *21*(4), 600–608. https://doi.org/10.1063/1.862268

Sergeev, V., Angelopoulos, V., Kubyshkina, M., Donovan, E., Zhou, X. Z., Runov, A., et al. (2011). Substorm growth and expansion onset as observed with ideal ground-spacecraft THEMIS coverage. *Journal of Geophysical Research*, *116*, A00I26. https://doi.org/10.1029/2010JA015689

Sergeev, V. A., Nikolaev, A. V., Kubyshkina, M. V., Tsyganenko, N. A., Singer, H. J., Rodriguez, J. V., et al. (2014). Event study combining magnetospheric and ionospheric perspectives of the substorm current wedge modeling. *Journal of Geophysical Research: Space Physics*, *119*, 9714–9728. https://doi.org/10.1002/2014JA020522

Sergeev, V. A., Nikolaev, A. V., Tsyganenko, N. A., Angelopoulos, V., Runov, A. V., Singer, H. J., & Yang, J. (2014). Testing a two-loop pattern of the substorm current wedge (SCW2L). *Journal of Geophysical Research: Space Physics*, *119*, 947–963. https://doi.org/10.1002/2013JA019629

Shore, R. M., Freeman, M. P., & Gjerloev, J. W. (2017). An empirical orthogonal function reanalysis of the northern polar external and induced magnetic field during solar cycle 23. *Journal of Geophysical Research: Space Physics*, *123*, 781–795. https://doi.org/10.1002/2017JA024420

Stauning, P. (2002). Field-aligned ionospheric current systems observed from Magsat and Oersted satellites during northward IMF. *Geophysical Research Letters*, *29*(15), 8005. https://doi.org/10.1029/2001GL013961

Stauning, P., Christiansen, F., & Watermann, J. (2005). Detection of Intense Fine-Scale Field-Aligned Current Structures in the Cusp Region. In C. Reigber, et al. (Eds.), *Earth observation with CHAMP*. Berlin: Springer.

Streltsov, A. V., & Lotko, W. (2004). Multiscale electrodynamics of the ionosphere-magnetosphere system. *Journal of Geophysical Research*, *109*, A09214. https://doi.org/10.1029/2004JA010457

Streltsov, A. V., & Lotko, W. (2008). Coupling between density structures, electromagnetic waves and ionospheric feedback in the auroral zone. *Journal of Geophysical Research*, *113*, A05212. https://doi.org/10.1029/2007JA012594

Streltsov, A. V., Pedersen, T. R., Mishin, E. V., & Snyder, A. L. (2010). Ionospheric feedback instability and substorm development. *Journal of Geophysical Research*, *115*, A07205. https://doi.org/10.1029/2009JA014961

Tanskanen, E. I., Pulkkinen, T. I., Viljanen, A., Mursula, K., Partamies, N., & Slavin, J. A. (2011). From space weather toward space climate time scales: Substorm analysis from 1993 to 2008. *Journal of Geophysical Research*, *116*, A00I34. https://doi.org/10.1029/2010JA015788

Tanskanen, E. I., Snekvik, K., Slavin, J. A., Perez-Suarez, D., Viljanen, A., Goldstein, M. L., et al. (2017). Solar cycle occurrence of Alfvenic fluctuations and related geo-efficiency. *Journal of Geophysical Research: Space Physics*, *122*, 9848–9857. https://doi.org/10.1002/2017JA024385

Trakhtengerts, V. Y., & Feldstein, A. Y. (1991). Turbulent Alfven boundary-layer in the polar ionosphere:1. Excitation conditions and energetics. *Journal of Geophysical Research*, *96*(A11), 19,363–19,374. https://doi.org/10.1029/91JA00376

Vasyliunas, V. M. (1970). Relation of plasma sheet to auroral oval. *Eos, Transactions American Geophysical Union*, *51*(11), 814.

Walsh, A. P., Haaland, S., Forsyth, S., Keesee, A. M., Kissinger, J., Li, K., et al. (2014). Dawn–dusk asymmetries in the coupled solar wind–magnetosphere–ionosphere system: A review. *Annales Geophysicae*, *32*, 705–737. https://doi.org/10.5194/angeo-32-705-2014

Wang, H., Luhr, H., & Ma, S. Y. (2005). Solar zenith angle and merging electric field control of field-aligned currents: A statistical study of the Southern Hemisphere. *Journal of Geophysical Research*, *110*, A03306. https://doi.org/10.1029/2004JA010530

Watermann, J., Stauning, P., Lühr, H., Newell, P. T., Christiansen, F., & Schlegel, K. (2009). Are small-scale field-aligned currents and magnetosheath-like particle precipitation signatures of the same low-altitude cusp? *Advances in Space Research*, *43*(1), 41–46. https://doi.org/10.1016/j.asr.2008.03.031

Waters, C. L., Anderson, B. J., & Liou, K. (2001). Estimation of global field aligned currents using the Iridium(R) system magnetometer data. *Geophysical Research Letters*, *28*(11), 2165–2168. https://doi.org/10.1029/2000GL012725

Weimer, D. R. (1994). Substorm time constants. *Journal of Geophysical Research*, *99*(A6), 11,005–11,015. https://doi.org/10.1029/93JA02721

Weimer, D. R. (1995). Models of high-latitude electric potentials derived with a least error fit of spherical harmonic coefficients. *Journal of Geophysical Research*, *100*(A10), 19,595–19,607. https://doi.org/10.1029/95JA01755

Weimer, D. R. (2001). Maps of ionospheric field-aligned currents as a function of the interplanetary magnetic field derived from Dynamics Explorer 2 data. *Journal of Geophysical Research*, *106*(A7), 12,889–12,902. https://doi.org/10.1029/2000JA000295

Wu, J., Bryant, M. S., Ridley, C. G., Shen, Y., Yang, L., Clausen, L. B. N., et al. (2017). A comparison of small-scale magnetic fluctuations in the Region 1 and 2 field-aligned current systems. *Journal of Geophysical Research: Space Physics*, *122*, 3277–3290. https://doi.org/10.1002/2016JA023453

Zhang, S.-R., Holt, J. M., & McCready, M. (2007). High latitude convection based on long-term incoherent scatter radar observations in North America. *Journal of Atmospheric and Solar-Terrestrial Physics*, *69*, 1273–1291. https://doi.org/10.1016/j.jastp.2006.08.017

Zhang, X.-J., Angelopoulos, V., Runov, A., Zhou, X.-Z., Bonnell, J., McFadden, J. P., et al. (2011). Current carriers near dipolarization fronts in the magnetotail: A THEMIS event study. *Journal of Geophysical Research*, *116*, A00I20. https://doi.org/10.1029/2010JA015885

Zhao, H., & Zong, Q. G. (2012). Seasonal and diurnal variation of geomagnetic activity: Russell-McPherron effect during different IMF polarity and/or extreme solar wind conditions. *Journal of Geophysical Research*, *117*, A11222. https://doi.org/10.1029/2012JA017845